Electrochemical impedance spectroscopy modeling using the distribution of relaxation times and error analysis for fuel cells

Vitor V. Lopes*, C. M. Rangel and Augusto Q. Novais

LNEG – National Laboratory for Energy and Geology, Estrada do Paço do Lumiar, 22, 1649-038 Lisboa, Portugal

(*) e-mail corresponding author: vitor.lopes@lneg.pt

Abstract

This paper proposes a new approach to determine the distribution of relaxation times (DRT) directly from the electrochemical impedance spectroscopy (EIS) data, i.e. without the use of an equivalent electrical circuit model. The method uses a generalized fractional-order Laguerre basis to represent EIS where both the parameters of the basis and their coefficients are estimated by solving a nonconvex minimization problem. Furthermore, the DRT confidence region is determined to assess the accuracy and precision of the DRT estimate. The approach is applied to analyze the dominant dynamic properties of an open-cathode hydrogen fuel-cell under different current and air-flow conditions. Results showed that the estimated DRT closely reconstructs EIS data even when there is a higher variance at smaller relaxation times.

Keywords: *Fuel-cell, impedance spectroscopy, distribution of relaxation times,parameter estimation, residuals bootstrap*

1 Introduction

Hydrogen polymer electrolyte fuel cells (PEMFC) are a strong alternative for developing high-energy density generation systems that can be both efficient and enviromental friendly. However, their performance depends on the mass transport phenomena inside the cell and the catalyst reaction kinetics, together with their coupling effects.

Electrochemical impedance spectroscopy (EIS) is commonly used as a base diagnostic technique because it retrieves information about the frequency response characteristics of the electrochemical system, but its direct use is limited. The usual approach to address EIS data is based on the development of models to represent the electrochemical phenomena. The modeling step is based on the use of equivalent electric circuits as a mathematical representation of the process in the Laplace domain.

Although this approach is widely used in the analysis of EIS data, it needs an informed insight on the nature of the phenomena inside the electrochemical cells. An alternative can be devised by using the distribution of relaxation times (DRT), which can be directly linked with the impedance spectrum through the Hilbert transform. Determining the DRT using impedance data requires the solution of a Fredholm integral equation of the first kind known as an ill-posed inverse problem. Although other approaches exist in the literature [1], we propose the use of a general fractional-order Laguerre basis for the representation of EIS data. First, the Laguerre basis is optimized by solving a nonconvex optimization problem. Then, the DRT is computed in two steps: i) solving the integral equation for each basis function, and ii) multiplying the linear combination coefficients by the corresponding DRT images of base functions to get the overall DRT.

The accuracy and precision of the DRT estimates was assessed using the residuals bootstrap method [2], modified to take into account the frequency dependency of the EIS error.

2 Experimental

An eight-cell stack, with an active area of 3.8 cm^2, was employed using a commercial catalyst coating membrane (3M) and GDL (gas diffusion layer, Johnson Matthey). Bipolar plates were made of graphite from Schunk, with anode flow fields having a proprietary design. The stack has an open-cathode with vertical channels. An air fan is located at the edge of the manifolds providing high stoichiometry oxidant supply and stack cooling. A purpose-built fuel cell testing station was used to control the inlet temperature, pressure and flow rate for the anode gas stream. Impedance measurements were carried out using a Solartron Frequency Response Analyser Model 1260. The frequency was typically spanned between 20 kHz and 0.1 Hz. The EIS dataset was collected under a fixed hydrogen flow-rate (0.4 $Lmin^{-1}$) and pressure (0.5 bar) by changing: a) the air flow-rate (2.4, 4.6, 8.0 $Lmin^{-1}$) with a fixed current of 0.5A; and, b) the current (0.35A, 0.5A, 1.0A) for a fixed air flow-rate of 8.0 $Lmin^{-1}$.

3 Estimation of the DRT and error analysis

3.1 Modeling the distribution of relaxation times

The method proposed for the analysis of impedance data is based on the concept of DRT [3]. The relation between the impedance $Z(jw)$ and its related distribution $G(\tau)$ of relaxation times τ is given by the following complex-valued integral:

$$\mathrm{Z(jw)} = \int_0^\infty \frac{\mathrm{G(\tau)}}{1+\mathrm{jw\tau}}\mathrm{d\tau} \quad (1)$$

where j is the complex unit and w is the frequency. The impedance Z(jw) of a relaxation process is usually represented by a peak in the $\mathrm{G}(\tau)$.

Impedance of a linear, time-invariant and casual system is uniquely characterized by the real part $\mathrm{Re\{Z(jw)\}}$ or the imaginary part $\mathrm{Im\{Z(jw)\}}$ of the transfer function (Kramers-Kronig relations). The integral of the distribution function over the whole domain is equal to the DC gain of the transfer function $Z(jw)$, i.e. $\int G(\tau)\, d\tau = \lim_{w\to 0} Z(jw)$. For a non-resonant system, $G(\tau)$ is truly a density distribution function since it is always positive. Note that the mathematical relation defined by equation (1) is valid even if $\mathrm{G}(\tau)$ takes negative values.

The impedance spectrum of real electrochemical systems is commonly modelled by equivalent electric circuits with components displaying a fractional order dependency on frequency [4]. This motivates the use of generalized fractional-order basis to describe the impedance spectrum [5], [6]. Let the fractional-order Laguerre base function be defined as [7]:

$$F_{l,m}(s) = \frac{1}{(s^\alpha+\lambda_m)^l} \quad (2)$$

where s is the Laplace variable, $\lambda_m \in \mathbb{R}$ is the parameter for adjusting base poles and α is the base fractional order, common to all base functions. The stability condition requires that $0 < \alpha < 2$ and all the base poles p_i must be in the region where $|\arg(p_i)| > \alpha\frac{\pi}{2}$. Unlike the rational case, the stability condition does not guarantee a fractional function to belong to the $H_2(\mathbb{C}^+)$ Hardy space, i.e. $F(s)$ is analytic on the open right half-plane $\mathbb{C}^+$ so that $\|F\|_2^2 = \int_{-\infty}^{\infty} F(jw)\,\overline{F(jw)}dw < \infty$. This condition is satisfied by imposing that the minimum degree for the base l satisfies the condition:

$$l \geq l_{min} = \left\lfloor \frac{1}{2\alpha} \right\rfloor + 1 \quad (3)$$

Where the function $\lfloor x \rfloor$ returns the largest integer not greater than x. For each Laguerre basis, it is possible to compute the associated distribution of relaxation times by solving equation (1) analytically using:

$$G_{l,m}(\tau) = -\lim_{\varepsilon\to 0^+} \frac{1}{\pi} Im\left\{F_{l,m}\left(-\frac{1}{\tau} - j\varepsilon\right)\right\} \quad (4)$$

Note that for $\mathrm{l} = 1$, the associated DRT is the well known Cole-Cole distribution. So the use of the generalized Laguerre basis can be seen as an extension of the commonly used approach, which employs a number of resistances and constant phase elements connected in a Voigt-type-of electric circuit [8]. In general, the impedance function can be represented as a linear combination of the Laguerre functions:

$$Z(s) = R_\infty + \sum_{m=1}^{M}\sum_{l=l_{min}}^{L_m} R_{l,m}F_{l,m} \quad (5)$$

where M is the number of the different modes, L_m is the number of Laguerre basis for the m[th] mode and $R_{l,m}$ are the linear coefficient weights.

3.2 Parameter estimation

The approximation of the impedance data using the function defined in eq. 5 requires the solution of a nonlinear optimization problem. As a preliminary step, an estimate of the fractional order of the basis can be determined by using the technique proposed by [7]. This step is important since it allows to simplify the optimization by setting the value of l_{min}, i.e. $l_{min} > \frac{1}{2\alpha} + 1$. In this study, the minimum number of terms in the Laguerre basis is set to $l_{min} = 2$ and each mode will make use of a fixed number of basis functions, i.e. $L_m = 3$. The overall optimization problem is defined as follows:

$$\begin{aligned} min \quad & \sum_i e_i^H e_i + \left(Re\left(\tilde{Z}_N\right) - R_\infty\right)^2 \\ s.t. \quad & e_i = (\tilde{Z}_i - Z_i)/|Z_i| \\ & Z_i = R_\infty + \sum_1^M \sum_2^5 R_{l,m}F_{l,m}(jw_i) \\ & R_\infty > 0 \\ & \alpha_m > \frac{1}{2}\frac{1}{l_{min}} = \frac{1}{4} \\ & \lambda_m > 0 \end{aligned}$$

where e_i^H is the complex conjugate of the i[th] error e_i, $\bar{Z}_i$ are the N measured values of the impedance at the w_i frequency, ordered from lowest to highest, and M is the number of modes used. Note that the objective function is composed of two terms, i.e. the sum of a weighted error function with an additional term that relates the high-frequency impedance with the infinite frequency resistance. The presence of this additional term is relevant to minimize the DRT contribution to the resistance at very low relaxation times (high-frequencies). The number of variables in the optimization problem is equal to $4\mathrm{M} + 2$, i.e. R_∞, α, and, for each mode: $\mathrm{R_{l,m}}$, λ_m.

The problem was formulated using the CASaDi modelling framework [9] and the IPOPT interior point nonlinear solver [10]. It is a non-convex optimization problem and hence it converges to an optimal solution, which might not be the global.

3.3 Validation and error analysis

The degree of approximation to the impedance data is controlled by the number of terms in equation (5), i.e. the number of modes M and the number of basis in each mode L_m. The goal is to have a representation as accurate as possible of the impedance data, for the determination of the associated DRT. The quality of this operation can be validated by performing the reverse operation, i.e. reconstructing the impedance spectra using the DRT. This can be achieved numerically by solving Eq. 1 using the following two steps procedure: first compute the DRT for a given set of relaxation times and then integrate Eq. 1 for each frequency w_i. The integration must be computed with a high level of accuracy to ensure that any differences between the experimental impedance values and the reconstructed impedance are only due to the DRT function. As such, the number of integration points was set to 10000.

The determination of the DRT estimate variance is performed using the residual bootstrap technique. Broadly speaking, it allows to compute the

variance of the DRT directly by resampling the EIS errors. The possible dependency of the error with the frequency is taken into account by limiting the sampling procedure to a limited neighbourhood around the frequency of interest. The number of bootstrap estimates was fixed to 50.

4 Results and discussion

Fig. 1 shows the two Nyquist plots for different sets of conditions, i.e. changes in the air flow-rate (top) and current (bottom). Each curve set comprises the experimental data (cross) and each one of the EIS curves calculated from the 50 DRT bootstrap estimates (dotted), where high color saturation stands for the regions with a high point density. Broadly speaking, both pictures display the closest agreement between reconstructed EIS and data that is possible to achieve with the proposed approach. Further, it allows to picture the reconstructed EIS confidence regions and find out the frequency range where the estimate is weaker. For instance, this is clear for the 4.6 and 8.0 $Lmin^{-1}$ cases (top), and is the direct effect of the high variability present in the data (low-frequency range).

The proposed approach can be used to assess which experimental data points comply with the Krammers-Kronig relations, since any EIS calculated from a DRT automatically follows these relations, see eq. 1. Thus, a good agreement between the experimental data and the reconstructed EIS shows that DRT provides a valid representation for the data. Moreover, it will be possible to detect anomalous data points by examining the confidence regions in the Nyquist plot.

Fig. 2 and 3, displays the DRT for the three different levels of current and air flow-rates. Each curve set shows the 50 estimated DRT from the bootstrap procedure. In general, each curve can be interpreted as the superposition of different single peak constructs, because of the linearity of Eq. 1. Thus, each peak location is linked to a dominant relaxation time found in the data, and its area related to the process polarization resistance. As a result, the direct comparison of the DRT allows to analyze the EIS gathered for different experimental conditions. Both figures show the confidence regions for each case. As expected, they highlight that DRT uncertainty is high for larger values of relaxation times. In particular, the cases of 4.6 $Lmin^{-1}$ and 8.0 $Lmin^{-1}$ (Fig. 2) reflect the impact of the high variability associated with low frequency data. Note that mainly the DRT low-frequency components show a marked influence by the experimental data. For instance, in the 1.0 A case, the DRT presents a high variability region for large relaxation times that is not clear from the Nyquist plot (bottom) and, hence, in this range results should be interpreted with care.

Nyquist plots predominantly evidenced a typical cathode response while DRT exhibits deconvolution of various mass transfer limited processes that can be adjudicated to the cathode as well as the

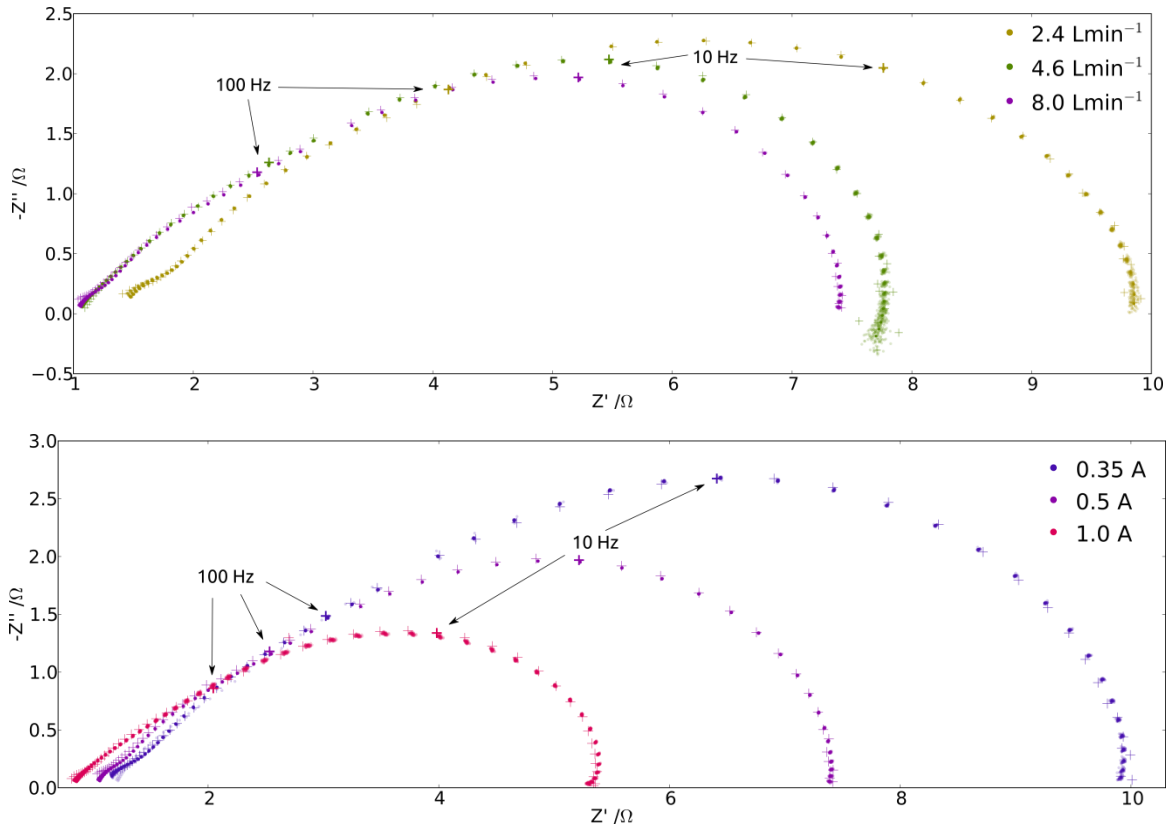

Fig. 1. Nyquist plot of the hydrogen fuel-cell EIS showing: the air flow effect for 2.4, 4.6 and 8.0 $Lmin^{-1}$ (up); and, the current effect for 0.35, 0.5 and 1.0 A (bottom). The cross represents the experimental data and the dots display the EIS computed from the DRT bootstraps. The dots have been plotted with a transparency level to highlight the accumulation of points on a given region – the more saturated the color is the higher probability.

anode. Membrane resistance is lowered with increased oxygen flow and increased current due to an increase in hydration by water formation. In genral, decrease in air supply causes an increase in the total resistance, more evident for the lower flow rate.

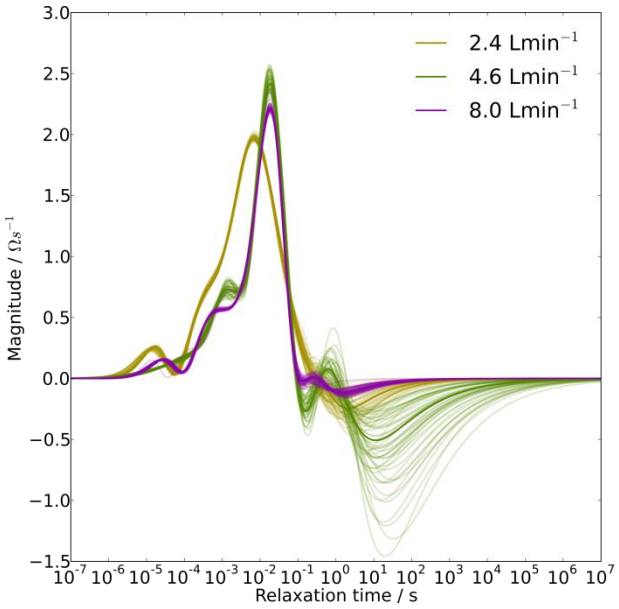

Fig. 2. DRT displays the air-flow effect upon the dynamic characteristics of the hydrogen fuel-cell. Each curve represents the DRT of a specific bootstrap.

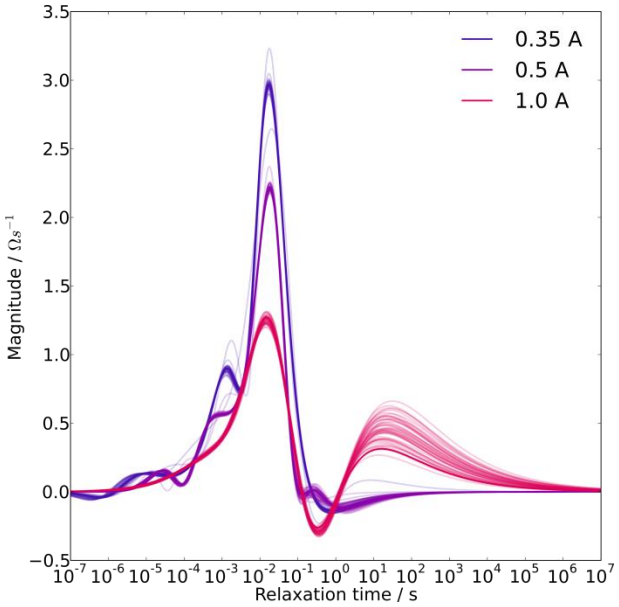

Fig. 3. DRT shows the effect of the current upon the dynamic characteristics of the hydrogen fuel-cell. Each curve represents the DRT of a specific bootstrap.

DRT analysis enabled the identification of limiting diffusion processes related to the presence of water in the porous media. Values of D_{eff}, the effective diffusivity, estimated from the DRT peak locations, were assigned to the catalyst layers-CL (water from the gas phase) and to the presence of water in the GDL/CL.

Low frequency inductive loops in impedance spectra are assumed to be associated with the adsorption of oxygen reduction reaction intermediaries. DRT related relaxation times takes negative values more evident in the low frequency boundary. This will be further discussed in terms of the response of physical processes occurring in the cell, since the analysis of errors in this work indicates that the low frequency region data is complyant with the Kramers-Kronig relations.

5 Conclusions

This paper proposes a novel method for the determination of the distribution of relaxation times directly from impedance spectroscopy data without the need to pre-specify an equivalent electric circuit impedance model. The reconstruction of the EIS spectrum from the DRT function allows validating both, i.e. the compliance of the EIS data with the Kramers-Kronig relations and the accurateness of the DRT representation.

6 References

[1] Schichlein, H., Müller, A. & Voigts, M. Deconvolution of electrochemical impedance spectra for the identification of electrode reaction mechanisms in solid oxide fuel cells. Journal of Applied Electrochemistry 32, 875–882 (2002).

[2] Lopes, V. V., Pinheiro, C. C. & Menezes, J. C. Determination of state-space model uncertainty using bootstrap techniques. Journal of Process Control 16, 685–692 (2006).

[3] Cole, K. S. & Cole, R. H. Dispersion and absorption in dielectrics I. Alternating current characteristics. The Journal of Chemical Physics 9, 341 (1941).

[4] Lopes, V. V., Rangel, C. M. & Novais, A. Q. Fractional-order transfer functions applied to the modeling of hydrogen PEM fuel cells. Computer Aided Chemical Engineering 1748–1752 (2011)

[5] Aoun, M., Malti, R., Levron, F. & Oustaloup, A. Synthesis of fractional Laguerre basis for system approximation. Automatica 43, 1640–1648 (2007).

[6] Malti, R., Aoun, M. & Oustaloup, A. Synthesis of fractional kautz-like basis with two periodically repeating complex conjugate modes. First International Symposium on Control, Communications and Signal Processing, 2004. 835-839

[7] Ghanbari, M. & Haeri, M. Order and pole locator estimation in fractional order systems using Bode diagram. Signal Processing 91, 191–202 (2011).

[8] Haschka, M. A direct approximation of fractional Cole-Cole systems by ordinary first-order processes. Advances in fractional calculus 257–270 (2007)

[9] Andersson, J. & Houska, B. Towards a computer algebra system with automatic differentiation for use with object-oriented modelling languages. Object-Oriented Modeling Languages 99–105 (2010)

[10] Wächter, A. & Biegler, L. T. On the implementation of an interior-point filter line-search algorithm for large-scale nonlinear programming. Mathematical Programming 106, 25–57 (2006).